

Toroidal Vortex Filament Knots & Links: Existence, Stability and Dynamics

T. Kolokolnikov,^{1,*} Christopher Ticknor,^{2,†} and P. G. Kevrekidis^{3,‡}

¹*Department of Mathematics and Statistics, Dalhousie University Halifax, Nova Scotia, B3H3J5, Canada*

²*Theoretical Division, Los Alamos National Laboratory, Los Alamos, New Mexico 87545, USA*

³*Department of Mathematics and Statistics, University of Massachusetts, Amherst, Massachusetts 01003-4515 USA*

(Dated: December 12, 2019)

Using the Klein-Majda-Damodaran model of nearly-parallel vortex filaments, we construct vortex knots and links on a torus involving periodic boundary conditions and analyze their stability. For a special class of vortex knots – toroidal knots – we give a full characterization of both their energetic and dynamical stability. In addition to providing explicit expressions for the relevant waveforms, we derive explicit formulas for their stability boundaries. These include simple links and different realizations of a trefoil knot. It is shown that a ring of more than 7 filaments can potentially be stabilized by giving it a slight twist and connecting neighbouring filaments on a torus. In addition to rings, (helical) filament lattice configurations are also considered and are found to be dynamically stable for all rotation frequencies and also energetically stable for sufficiently fast rotations. Numerical simulations are used to compare the Klein-Majda-Damodaran model with the full three-dimensional (3D) Gross-Pitaevskii equations as well as to confirm the analytical theory. Potential differences between the quasi-one-dimensional and the fully 3D description are also discussed.

1. INTRODUCTION

States bearing topological charge constitute a principal theme within a variety of areas in Physics, including (but not limited to) optics [1], condensed matter [2, 3], as well as hydrodynamics [4]. The experimental realization of Bose-Einstein condensates (BECs) has offered a platform where numerous vortical excitations could be explored, and their interactions with each other and with external potential landscapes could be monitored in a systematic, time-resolved manner [5–7]. This has led to a significantly enhanced understanding of the role of vortical patterns in BEC dynamics, as well as in quantum turbulence, which has by now been summarized in a substantial number of review publications [8–13].

The gradual formulation of an understanding of the building blocks such as vortex lines and vortex rings as summarized in the above studies has propelled a considerable volume of ongoing interest towards the formulation, dynamical monitoring and qualitative understanding of more elaborate structures such as vortex knots and links. These have been explored chiefly in a homogeneous (density background) setting as, e.g., in [14–22]. Recent work [23] has argued that upon suitable (anisotropic) trapping conditions such knot structures may be long-lived, while experiments with spinor BECs have spearheaded the realization/observation of the structures [24, 25]. It is worth noting, in passing, that such structures are not only relevant in BECs but in numerous other areas including, e.g., nonlinear optics [26], but also DNA strands [27], magnetic fields in plasmas [28], classical fluids [29], superfluids [30, 31]; and helical filaments in the wake of turbines [32–35].

Our starting point in the present work will be rather different than that of most of the above studies. We will start from an effective quasi-one-dimensional mathematical description of vortex filaments developed in [36] (see also [37] for an equilibrium statistical theory and [38] for a recent dynamical analysis of the model). We will use the latter as a framework for obtaining exact analytical solutions for co-rotating (helical) vortex filaments. The latter through the use of periodic boundary conditions will formulate structures akin to vortical knots and links. Upon identifying such states and parametrizing them by a pair of integer indices, we will analyze their existence (e.g. frequency and radius of rotation in section 2), as well as stability (in section 3) properties. In section 4, we examine a lattice of such filaments. In section 5, we return to the original motivating problem of the 3-dimensional prototypical model of BECs (the Gross-Pitaevskii (GP) equation [5–7]) and explore the validity of our existence and stability conclusions therein. Finally, we summarize our findings and present our conclusions, as well as some possible directions of future study in section 6.

* tkokolokol@gmail.com

† cticknor@lanl.gov

‡ kevrekid@umass.edu

2. EXISTENCE OF VORTEX FILAMENT STATES

In [36, 37] the authors derived a simplified model describing the evolution of K nearly-parallel vortex filaments – the so-called Klein–Majda–Damodaran (KMD) model. The reduced equations they derived are

$$-i\frac{\partial}{\partial t}X_k = D\frac{\partial^2}{\partial z^2}X_k + \sum_{j \neq k} \frac{X_k - X_j}{|X_k - X_j|^2}, \quad k = 1 \dots K. \quad (2.1)$$

Here, z denotes the direction that is nearly parallel to all the filaments; and $X_k(z, t) \in \mathbb{R}^2$ is the two-dimensional position of the k -th (topologically charged) filament at height z and time t .

The goal of this paper is to study the stability of helical “co-rotating” vortex filaments using the reduced equations (2.1). We also, however, endeavor to return to the original Gross-Pitaevskii model from which this reduced dynamics is obtained and to compare the predictions of the effective model with the original one. We assume that each filament is rotating with the same angular velocity Ω without changes in shape, so that the whole configuration undergoes a “rigid” rotation. These are some of the simplest nontrivial filament configurations. By analogy to point vortex literature, we refer to these configurations as *relative equilibria* [39–42], i.e., equilibria in the rotational frame of reference. Assuming that the system rotates with a rate Ω , we make a change of variables

$$X_k(z, t) = e^{i\Omega t}\xi_k(z, t) \quad (2.2)$$

so that the ξ_k satisfy

$$-i\frac{\partial}{\partial t}\xi_k = D\frac{\partial^2}{\partial z^2}\xi_k - \Omega\xi_k + \sum_{j \neq k} \frac{\xi_k - \xi_j}{|\xi_k - \xi_j|^2}. \quad (2.3)$$

Relative equilibria are time-independent steady states of this system. More generally, we also examine what happens when adding “relaxation” as follows:

$$(-i\gamma_1 + \gamma_2)\frac{\partial}{\partial t}\xi_k = D\frac{\partial^2}{\partial z^2}\xi_k - \Omega\xi_k + \sum_{j \neq k} \frac{\xi_k - \xi_j}{|\xi_k - \xi_j|^2}. \quad (2.4)$$

The latter model has been used in the context of vortices in order to study their dynamics in finite temperature settings [43, 44] and relevant ideas have even been extended to recent experiments measuring, e.g., the rate of vortex spiraling out of the condensate in connection with the relaxational term in the corresponding dynamics [45]. The limit $\gamma_1 \rightarrow 0$ (or $\gamma_2 \rightarrow \infty$) can be thought of as an overdamped limit. After time-rescaling, the overdamped system leads to

$$\frac{\partial}{\partial t}\xi_k = D\frac{\partial^2}{\partial z^2}\xi_k - \Omega\xi_k + \sum_{j \neq k} \frac{\xi_k - \xi_j}{|\xi_k - \xi_j|^2}. \quad (2.5)$$

The equilibrium (time-independent) configurations are solutions of the system (2.4); at the same time they are also steady states for both (2.3) and (2.5). However it turns out that the stability of the two systems (2.3) and (2.5) can be different. We shall refer to stability with respect to (2.5) as **energetic stability**; whereas the stability with respect to (2.3) will be called **dynamical stability**. This nomenclature is justified by thinking of (2.5) as the gradient flow of the associated energy functional discussed, e.g., in [36, 38]. We will show that there are *stable* equilibrium solutions of (2.3) which are unstable with respect to the system (2.5). This is a feature that is common in Hamiltonian systems in connection to their dissipative counterparts; see, e.g., [46] for a relevant discussion of dynamical and energetic stability.

The questions that we ask are the following:

- What are the steady states of (2.3)?
- What is their dynamical stability (i.e. stability with respect to (2.3))?
- What is their energetic stability (i.e. stability with respect to (2.5))?

The stability is intimately connected with the selection of boundary conditions. In this work we assume the following *doubly-periodic boundary conditions*

$$z \in [0, P]; \quad \xi_k(P, t) = \xi_{k+q}(0, t) \pmod{K}. \quad (2.6)$$

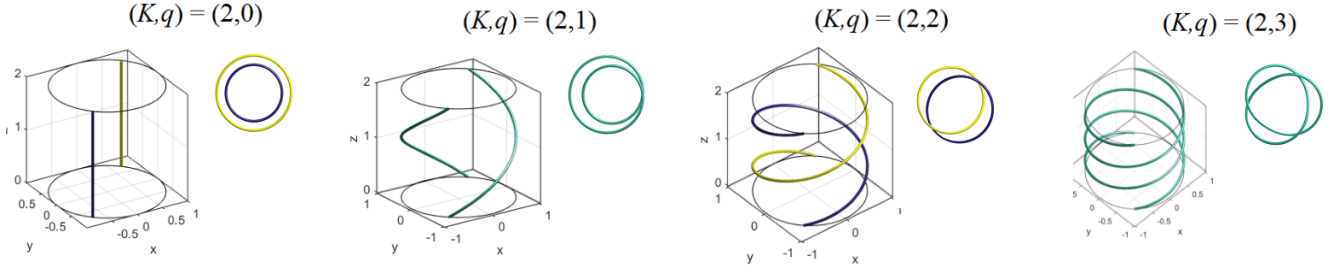


FIG. 1. Two graphical representations of toroidal vortex filament knots for several values of (K, q) as indicated. On the left is the cartesian representation with $(x, y) = \xi_k(z)$. On the right is toroidal representation with z wrapping around the center of the torus. Refer also to Table I

The “usual” periodic BC correspond to the case where q is an integer multiple of K . When visualized on a torus, such doubly-periodic solutions represent knots and links (with the number of links being given by the $\text{gcd}(K, q)$). The simplest such knots and links, corresponding to helical filaments, are the so-called *toroidal* knots, and are illustrated in Figure 1; see also Table I below. For example the trefoil knot can be realized as a $(K, q) = (2, 3)$ toroidal knot.

The simplest configuration consists of straight filaments, where each z cross-section corresponds to point vortices in a relative equilibrium. The corresponding dynamics is that of co-rotating 2D vortices, trivially extended into the third dimension. As we will show below, these structures are dynamically stable with respect to the reduced equations (2.1), as long as the underlying point vortex configuration is stable.

A more interesting steady state consists of helical filaments having the form

$$\xi_k(t, z) = e^{zi\omega} \eta_k \quad (2.7)$$

with η_k satisfying

$$0 = -\Gamma \eta_k + \sum_{j \neq k} \frac{\eta_k - \eta_j}{|\eta_k - \eta_j|^2} \quad \text{where} \quad \Gamma = D\omega^2 + \Omega. \quad (2.8)$$

In other words, $\{\eta_k\}, k = 1 \dots K$ are relative equilibria of the associated point-vortex problem, corresponding to a shifted frequency $\Gamma = \Omega + D\omega^2$. Conversely, all helical filament states of the form (2.7) correspond to equilibria of the point-vortex problem (2.8). Note also that Γ in (2.8) can be set to one by rescaling, so that this problem is parameter-free.

We remark that the solution to (2.8) exists only if $\Gamma > 0$ [47]. To see this, take the dot product of (2.8) with η_k and sum over k . We then obtain

$$\Gamma \sum_k |\eta_k|^2 = \sum_k \sum_{j \neq k} \frac{|\eta_k|^2 - \eta_j \cdot \eta_k}{|\eta_k - \eta_j|^2} = \sum_k \sum_{j > k} \frac{|\eta_k|^2 - 2\eta_j \cdot \eta_k + |\eta_j|^2}{|\eta_k - \eta_j|^2} = \frac{(K-1)K}{2},$$

so that

$$\Gamma = \frac{(K-1)K}{2} \frac{1}{\sum_k |\eta_k|^2} > 0. \quad (2.9)$$

A natural realization of the boundary conditions (2.6) is by placing vortices uniformly along a ring,

$$\eta_k = r e^{i2\pi k/K} \quad (2.10)$$

while setting the frequency ω in (2.7) to be

$$\omega = \frac{2\pi}{P} \frac{q}{K}, \quad q \in \mathbb{Z}, \quad (2.11)$$

so that the doubly-periodic boundary conditions are automatically satisfied. Then we have

$$\sum_{j \neq k} \frac{\eta_k - \eta_j}{|\eta_k - \eta_j|^2} = \frac{e^{i2\pi k/K} (K-1)}{r} \frac{1}{2},$$

so that r is given by

$$r^2 = \frac{K-1}{2\Gamma} \quad (2.12)$$

(as can also be seen from (2.9)). This leads to what we shall call a filament ring state:

Proposition 2.1. ((K, q) filament ring). *For any integers q, K , there is a steady state of (2.5) that has the form*

$$\xi_k(t, z) = r e^{zi\omega} e^{i2\pi k/K} \quad (2.13)$$

where

$$\omega = \frac{2\pi q}{P K}, \quad r^2 = \frac{K-1}{2(D\omega^2 + \Omega)} \quad (2.14)$$

Such a steady state satisfies the boundary conditions $\xi_k(P) = \xi_{k+q}(0)$ where the indices are taken modulo K .

Figure 1 and Table I show some case examples of these steady states. We now provide the layout of the results that follow. Firstly, we give the full characterization of stability of these filament rings, both energetic and dynamical. This is done in Section 3. We then consider more general helical states where each z-cross-section is a steady state corresponding to (2.8). We refer to such a state as a helical filament lattice. For a general vortex lattice that is not on a ring, we consider only periodic boundary conditions (so that q is a multiple of K in (2.7, 2.6, 2.11)). In Section 4 we show that such a filament lattice is dynamically stable, provided that the underlying vortex lattice is stable. However it can become energetically unstable for sufficiently small Ω . Some direct numerical simulations of the proposed equilibria are given in 5, exploring our findings in the full 3D model, before raising some questions for future study in Section 6.

3. STABILITY OF FILAMENT RING STATES

To analyze the ring stability, we deploy the complex variables-based technique of [48, 49] in order to examine the circular Fourier modes of a ring. We start with a general perturbation of the (K, q) ring state as follows:

$$\xi_k(t, z) = e^{i2\pi k/K} (e^{i\omega z} r + \phi_k(t, z)), \quad \phi_k \ll 1. \quad (3.15)$$

This yields the following linear system for ϕ_k :

$$(-i\gamma_1 + \gamma_2) \phi'_k = (D\partial_{zz} - \Omega) \phi_k + e^{i\omega z} \sum_{j \neq k} \frac{1}{r^2} \frac{1}{4 \sin^2(\pi(j-k)/K)} (\exp(2\pi i(j-k)/K) \bar{\phi}_k - \bar{\phi}_j).$$

Next, we decompose the perturbation into Fourier modes using the following self-consistent ansatz:

$$\phi_k = e^{i(\alpha+\omega)z} e^{2\pi imk/K} \phi_+(t) + e^{i(-\alpha+\omega)z} e^{-2\pi imk/K} \bar{\phi}_-(t). \quad (3.16)$$

Collecting the like terms in $e^{i(\alpha+\omega)z} e^{2\pi imk/K}$ and $e^{i(-\alpha+\omega)z} e^{-2\pi imk/K}$ yields a 2x2 system:

$$\begin{aligned} (-i\gamma_1 + \gamma_2) \phi'_+ &= \left(-D(\alpha + \omega)^2 - \Omega \right) \phi_+ + \sigma_+ \phi_- \\ (+i\gamma_1 + \gamma_2) \phi'_- &= \left(-D(\omega - \alpha)^2 - \Omega \right) \phi_- + \sigma_+ \phi_+ \end{aligned}$$

where

$$\sigma_{\pm} = \sum_{j=1}^{K-1} \frac{1}{r^2} \frac{1}{4 \sin^2(\pi j/K)} (\exp(2\pi i j/K) - \exp(\pm 2\pi i j m/K)). \quad (3.17)$$

Using identities from [48] (see (3.8) there), we obtain

$$\sigma_+ = \sigma_- = \sigma = \frac{1}{2r^2} (m-1)(K-m-1). \quad (3.18)$$

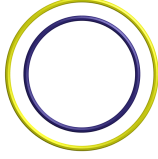
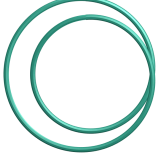
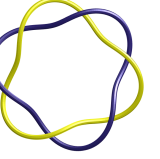
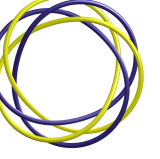
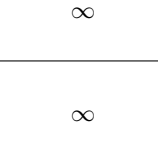
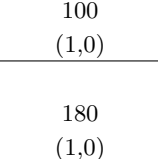
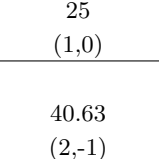
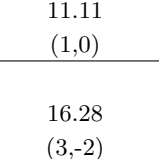
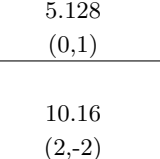
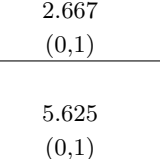
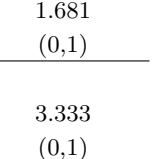
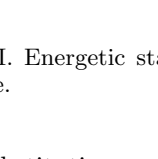
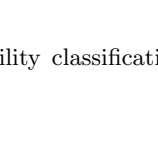
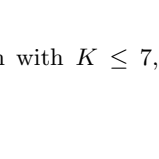
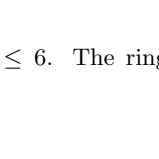
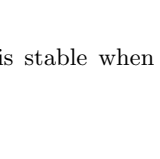
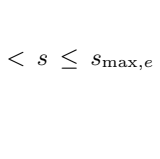
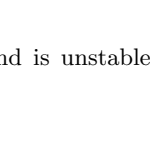
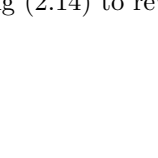
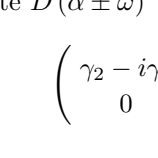
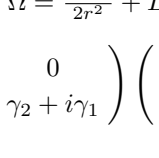
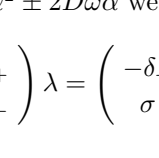
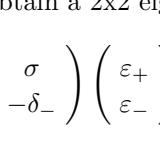
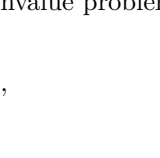
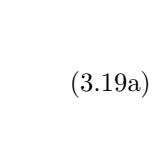
	$q = 0$	$q = 1$	$q = 2$	$q = 3$	$q = 4$	$q = 5$	$q = 6$
$K = 2$							
$s_{\max,e}$	∞	4	0.6667	0.25	0.1333	0.08333	0.05714
(m, M)		(1,0)	(0,1)	(0,1)	(0,1)	(0,1)	(0,1)
$K = 3$							
$s_{\max,e}$	∞	18	4.5	1.333	0.6545	0.3956	0.2667
(m, M)		(1,0)	(1,0)	(0,1)	(0,1)	(0,1)	(0,1)
$K = 4$							
$s_{\max,e}$	∞	48	12	4.8	2	1.143	0.75
(m, M)		(1,0)	(1,-1)	(0,1)	(0,1)	(0,1)	(0,1)
$K = 5$							
$s_{\max,e}$	∞	100	25	11.11	5.128	2.667	1.681
(m, M)		(1,0)	(1,0)	(1,0)	(0,1)	(0,1)	(0,1)
$K = 6$							
$s_{\max,e}$	∞	180	40.63	16.28	10.16	5.625	3.333
(m, M)		(1,0)	(2,-1)	(3,-2)	(2,-2)	(0,1)	(0,1)
$K = 7$							
$s_{\max,e}$	∞	294	39.2	18.38	9.8	5.939	4.356
(m, M)		(1,0)	(3,-1)	(3,-1)	(3,-2)	(3,-2)	(3,-3)

TABLE I. Energetic stability classification with $K \leq 7, q \leq 6$. The ring is stable when $0 < s \leq s_{\max,e}$ and is unstable otherwise.

Upon substituting

$$\phi_{\pm}(t) = e^{\lambda t} \varepsilon_{\pm}$$

and using (2.14) to rewrite $D(\alpha \pm \omega)^2 + \Omega = \frac{K-1}{2r^2} + D\alpha^2 \pm 2D\omega\alpha$ we obtain a 2x2 eigenvalue problem

$$\begin{pmatrix} \gamma_2 - i\gamma_1 & 0 \\ 0 & \gamma_2 + i\gamma_1 \end{pmatrix} \begin{pmatrix} \varepsilon_+ \\ \varepsilon_- \end{pmatrix} \lambda = \begin{pmatrix} -\delta_+ & \sigma \\ \sigma & -\delta_- \end{pmatrix} \begin{pmatrix} \varepsilon_+ \\ \varepsilon_- \end{pmatrix}, \quad (3.19a)$$

$$\delta_{\pm} = \frac{K-1}{2r^2} + D\alpha^2 \pm 2D\omega\alpha. \quad (3.19b)$$

Next, recall that $\xi_k(P) = \xi_{k+q}(0)$. From (3.15), this implies that

$$\phi_k(P, t) = e^{i2\pi q/K} \phi_{k+q}(0, t)$$

so that

$$e^{i(\alpha+\omega)P} e^{2\pi imk/K} \phi_+(t) + e^{i(-\alpha+\omega)P} e^{-2\pi imk/K} \bar{\phi}_-(t) = e^{i2\pi q/K} \left(e^{2\pi im(k+q)/K} \phi_+(t) + e^{-2\pi im(k+q)/K} \bar{\phi}_-(t) \right). \quad (3.20)$$

Upon substituting $\omega P = 2\pi q/K$, we find that (3.20) is satisfied for all k if and only

$$\alpha/\omega = m + MK/q, \quad \text{where } M \in \mathbb{Z}. \quad (3.21)$$

We summarize these computations as follows.

Proposition 3.1. [General Stability Formulation]. *Consider the (K, q) ring state as given by Proposition 2.1. Its stability is determined by a sequence of 2×2 eigenvalue problems (3.19) where*

$$\delta_{\pm} = \frac{K-1}{2r^2} + D \left(\frac{2\pi}{P} \right)^2 \left(\frac{mq}{K} + M \right) \left(\frac{mq \pm 2q}{K} + M \right), \quad \sigma = \frac{1}{2r^2} (m-1)(K-m-1).$$

Here, m is the azimuthal mode between the K filaments, whereas M is the Fourier mode along each of the filaments, with the perturbation having the form

$$\phi_k(t, z) = \exp \left(i \frac{2\pi z}{P} \left(\frac{mq+q}{K} + M \right) + 2\pi imk/K \right) \phi_+(t) + \exp \left(i \frac{2\pi z}{P} \left(\frac{-mq+q}{K} - M \right) - 2\pi imk/K \right) \bar{\phi}_-(t). \quad (3.22)$$

We now apply this general formula to two specific cases, namely $\gamma_2 = 0$ to which we refer to as *dynamical stability* (for the Hamiltonian case) or $\gamma_1 = 0$ which we refer to as *energetic stability* (for the gradient system scenario).

3.1. Dynamical stability

To study dynamical stability (i.e. stability with respect to (2.3)), we set $\gamma_1 = 1, \gamma_2 = 0$ in Proposition 3.1. Then λ satisfies

$$\begin{pmatrix} \varepsilon_+ \\ \varepsilon_- \end{pmatrix} \lambda = \begin{pmatrix} \delta_+ i & \sigma i \\ -\sigma i & -\delta_- i \end{pmatrix} \begin{pmatrix} \varepsilon_+ \\ \varepsilon_- \end{pmatrix}. \quad (3.23)$$

so that

$$\lambda^2 - i(\delta_- - \delta_+) \lambda + (\delta_+ \delta_- - \sigma^2) = 0,$$

having two solutions,

$$\lambda_{\pm} = \frac{i}{2} (\delta_- - \delta_+) \pm \frac{1}{2} \sqrt{4\sigma^2 - (\delta_+ + \delta_-)^2}.$$

It follows that the filament ring is dynamically stable if and only if

$$|\sigma| \leq \frac{\delta_+ + \delta_-}{2}. \quad (3.24)$$

In this case, the eigenvalues λ_{\pm} are purely imaginary. Otherwise, the steady state has saddle structure (with $\text{Re}(\lambda_+) > 0$ and $\text{Re}(\lambda_-) < 0$). Recalling (3.18, 3.19c), the stability condition (3.24) is equivalent to:

$$K-1 + 2r^2 D \left(\frac{2\pi}{P} \right)^2 \left(\frac{mq}{K} + M \right)^2 \geq (m-1)(K-m-1), \quad \text{for all } m \in \{1 \dots K-1\}, M \in \mathbb{Z}. \quad (3.25)$$

We therefore define a dimensionless parameter

$$s := \left(\frac{2\pi}{P} \right)^2 2Dr^2. \quad (3.26)$$

so that (3.25) can be written as $s \geq \frac{K(m-2)-m^2+2}{\left(\frac{mq}{K}+M\right)^2}$. We summarize as follows.

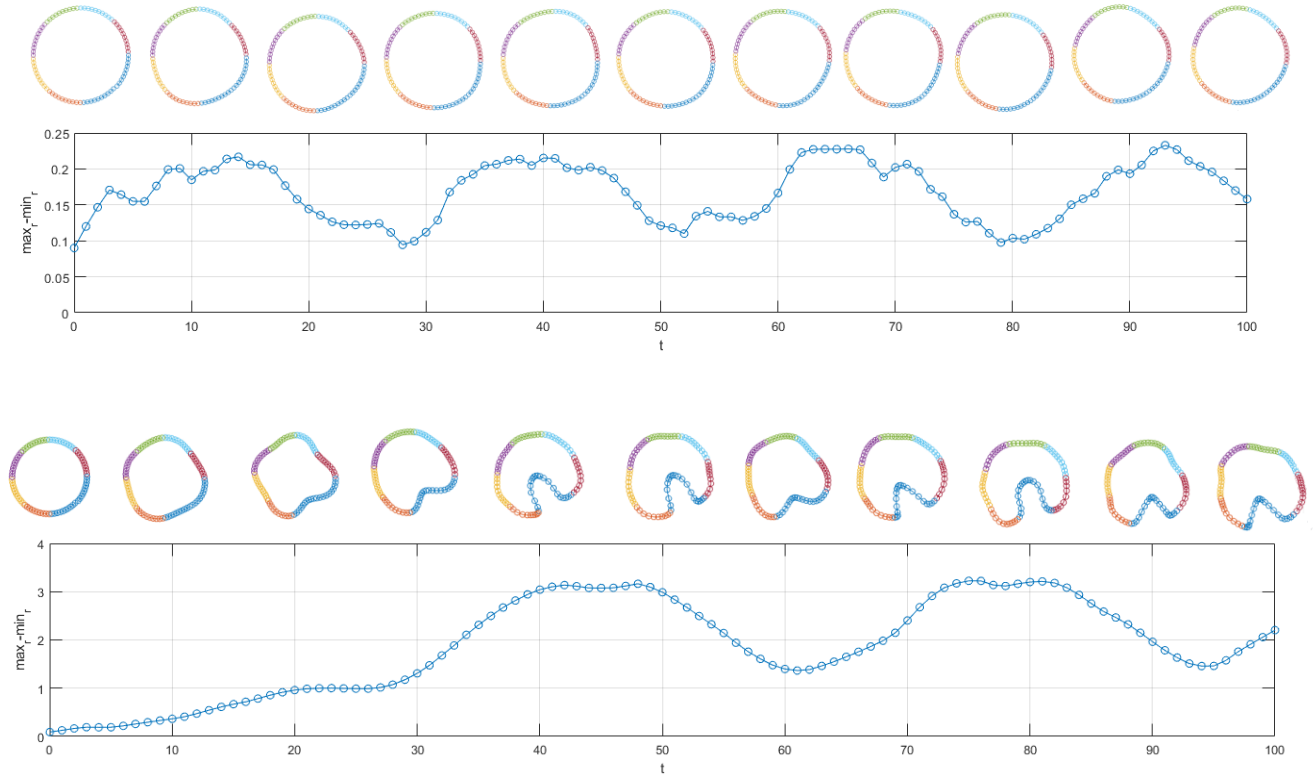


FIG. 2. Simulation of system (2.1) with $K = 8, q = 1, \gamma_1 = 1, \gamma_2 = 0, D = 1/2$. Top: $r = 3.0$ (stable regime). Bottom: $r = 2.5$ (unstable regime). The theoretical stability threshold is $r = \sqrt{8} = 2.828$. The vertical axis shows $\max |\xi| - \min |\xi|$, versus time t . Snapshots show the actual solution viewed from the top with $t = 0, 10, 20 \dots 100$, with different colours corresponding to different filaments. Initial conditions consist of the the steady state, slightly perturbed at $t = 0$. Note that the destabilizing mode $m = 4$ is clearly visible (bottom figure)

Theorem 3.2. [*Dynamical stability*]. *Let*

$$s_{\min,d} := \max_{\substack{m \in \{1 \dots K-1\}, \\ M \in \mathbb{Z}}} \frac{K(m-2) - m^2 + 2}{\left(\frac{mq}{K} + M\right)^2} \quad (3.27)$$

Then a (K, q) ring is **dynamically stable** provided that $s > s_{\min,d}$, where s is the dimensionless parameter given by (3.26).

There are several important subcases.

- **Case 1:** $K \leq 7$, **any** q . In this case, $K(m-2) - m^2 + 2 \leq 0$ for all $m \in \{0, \dots, K-1\}$ so that $s_{\min,d} \leq 0$, and it follows that a ring of $K \leq 7$ filaments is **dynamically stable** for all r .
- **Case 2:** $K \geq 8$ and $\gcd(q, K) \neq 1$. Then there are integers m, M with $m \in (1, K-1)$ such that $\frac{mq}{K} + M = 0$, while $K(m-2) - m^2 + 2 > 0$. This implies $s_{\min,d} = \infty$; hence the ring is **dynamically unstable** for any r .
- **Case 3:** $K \geq 8$, and $q = 1$. The most unstable mode turns out to be $(m, M) = (4, 0)$, with $s_{\min,d} = \left(\frac{K-7}{8}\right) K^2$. Note also that $s_{\min,d}$ does not change when adding any multiple of K to q . Therefore we may assume without loss of generality that $q \in \{0 \dots K-1\}$. Table II lists $s_{\min,d}$ the and associated destabilizing mode (m, M) for several values of K and q .

Example. Take $K = 8, q = 1$. Then $s_{\min,d} = 8$. Figure 2 shows the numerical simulations of (2.3), with s to either side of the stability boundary, in full agreement with the predicted stability.

$K = 8 :$	q	0	1	2	3	4	5	6	7	8			
	$s_{\min,d}$	∞	8	∞	64	∞	64	∞	8	∞			
	m	4	4	3	4	3	4	4					
	M	0	-1	-1	-2	-2	-3	-4					
$K = 9 :$	q	0	1	2	3	4	5	6	7	8	9		
	$s_{\min,d}$	∞	$20\frac{1}{4}$	324	∞	81	81	∞	324	$20\frac{1}{4}$	∞		
	m	4	4	3	4	4	3	4	4				
	M	0	-1	-1	-2	-2	-2	-3	-4				
$K = 10 :$	q	0	1	2	3	4	5	6	7	8	9	10	
	$s_{\min,d}$	∞	$37\frac{1}{2}$	∞	300	∞	∞	∞	300	∞	$37\frac{1}{2}$	∞	
	m	4	5	3	5	4	5	7	5	4			
	M	0	-1	-1	-2	-2	-3	-5	-4	-4			
$K = 11 :$	q	0	1	2	3	4	5	6	7	8	9	10	11
	$s_{\min,d}$	∞	$60\frac{1}{2}$	1210	968	484	242	242	484	968	1210	$60\frac{1}{2}$	∞
	m	4	6	4	3	7	4	3	4	5	7		
	M	0	-1	-1	-1	-3	-2	-2	-3	-4	-4	-6	

TABLE II. Dynamical stability for filament rings with $K = 8, 9, 10, 11$. Stability range is $s \geq s_{\min,d}$ where $s = \left(\frac{2\pi}{P}\right)^2 2Dr^2$.

3.2. Energetic stability

Energetic stability corresponds to the study of the eigenvalue problem (3.19a) with $\gamma_2 = 1, \gamma_1 = 0$. In this case, the eigenvalues are purely real since they are the eigenvalues of the symmetric matrix $\begin{pmatrix} -\delta_+ & \sigma \\ \sigma & -\delta_- \end{pmatrix}$. Moreover, the trace $-\delta_+ - \delta_-$ is negative, see (3.19c). It follows that the filament ring is dynamically stable if and only if determinant is positive, or

$$\sigma^2 \leq \delta_+ \delta_- . \quad (3.28)$$

Contrast this with the condition for dynamical stability (3.24): $|\sigma| \leq \frac{\delta_+ + \delta_-}{2}$. By the elementary inequality, $\sqrt{\delta_+ \delta_-} \leq \frac{\delta_+ + \delta_-}{2}$ for any $\delta_{\pm} > 0$, with equality if and only if $\delta_+ = \delta_-$, it immediately follows that **energetic stability implies dynamical stability**. The former is associated with the geometric mean of δ_+ and δ_- , while the latter with the arithmetic mean thereof. Of course the converse is false since in general, $\delta_+ \neq \delta_-$. (the exception is when either $q = 0$ or $m + MK/q = 0$).

Written in dimensionless variable $s = \left(\frac{2\pi}{P}\right)^2 2Dr^2$, the stability criterion (3.28) is equivalent to $\mu \geq 0$ where

$$\mu := \left[1 + \frac{s}{K-1} \left(\frac{mq}{K} + M \right) \left(\frac{mq+2q}{K} + M \right) \right] \left[1 + \frac{s}{K-1} \left(\frac{mq}{K} + M \right) \left(\frac{mq-2q}{K} + M \right) \right] - (m-1)^2 \left(1 - \frac{m}{K-1} \right)^2 , \quad (3.29)$$

with the stability boundary corresponding to $\mu = 0$. We summarize as follows.

Proposition 3.3. [Energetic stability]. *The (K, q) ring is energetically stable provided that $\mu \geq 0$ for all $m \in \{0, 1, \dots, K-1\}$ and all $M \in \mathbb{Z}$, with μ given by (3.29). It is unstable otherwise. A ring is dynamically stable if it is energetically stable (but the converse is not true in general).*

For further insight, first consider the case $s \rightarrow 0$. One can think of this as the limit where the Laplacian term in Eq. (2.3) is absent, as is the case, e.g., for point vortices (rather than filaments). Then,

$$\mu \sim 1 - \left((m-1) \left(1 - \frac{m}{K-1} \right) \right)^2 , \quad s = 0 \quad (3.30)$$

and the stability is independent of M or q . In this case, as is well-known for point vortices [50], the ring is stable if $K \leq 7$ and is unstable otherwise. So the case $K \leq 7$ and $K \geq 7$ must be analyzed separately.

K	8	9	10	11	12	20	50	100	200	$\gg 1$
$s_{\min,d}$	8	20.25	37.5	60.5	90	650	13437	116250	965000	$\sim 0.125K^3$
$s_{\min,e}$	8.234	21.164	39.564	64.237	96	703.7	14677	127276	1057677	$\sim 0.137K^3$
$s_{\max,e}$	448	648	900	1210	1584	7600	122500	990000	7960000	$\sim K^3$

TABLE III. Stability classification for $K > 7$, $q = 1$. The ring is energetically stable iff $s_{\max,e} \leq s \leq s_{\max,e}$. It is dynamically stable iff $s_{\min,d} \leq s$.

Next, consider the mode $(m, M) = (1, 0)$. Then μ simplifies to

$$\mu = \left(1 - s \frac{q^2}{(K-1)K^2}\right) \left(1 + 3s \frac{q^2}{(K-1)K^2}\right), \quad (m, M) = (1, 0). \quad (3.31)$$

Therefore this mode is unstable when $s > s_{(1,0)}$ where

$$s_{(1,0)} := \frac{(K-1)K^2}{q^2}. \quad (3.32)$$

In fact, from (2.14, 3.26) note that the rotation rate Ω can be written as $\Omega = \frac{2\pi}{P} D \left(\frac{K-1}{s} - \frac{q^2}{K^2} \right)$. Thus the threshold $s = (K-1)K^2/q^2$ corresponds *precisely* to the zero-rotation rate $\Omega = 0$.

Next, take $(m, M) = (0, 1)$ in which case we obtain

$$\mu = \frac{s}{(K-1)^2 K^2} [(K^2 - 4q^2)s + 2(K-1)K^2], \quad (m, M) = (0, 1) \quad (3.33)$$

When $q < K/2$, this mode is always stable. On the other hand, this mode is unstable if $q > K/2$ and $s > s_{(0,1)}$ where

$$s_{(0,1)} := \frac{2(K-1)K^2}{4q^2 - K^2} \quad (3.34)$$

A bit of algebra shows that $s_{(0,1)} < s_{(1,0)}$ whenever $K/2 < q < K/\sqrt{2}$.

Table III list the value of $s_{\max,e}$ and the corresponding mode (m, M) for $2 \leq K \leq 7$ and $0 \leq q \leq 6$. With some exceptions (such as $(K, q) = (6, 3)$ or $K = 7, q \geq 2$), the instability threshold corresponds to either $s_{(0,1)}$ or $s_{(1,0)}$.

Finally, consider the case $K > 7$. Then additional algebra shows that (K, q) with $q \neq 1$ is unstable for *all* $s \geq 0$. On the other hand, when $q = 1$, there exists a stability band $s_{\min,e} \leq s \leq s_{\max,e}$ where it is stable, while it is unstable outside this range. The upper bound corresponds to the mode $(m, M) = (1, 0)$ given by $s_{\max,e} = s_{(1,0)}$. On the other hand, additional computations reveal that the lower bound corresponds to the mode $(m, M) = (4, 0)$. Upon substituting $(m, M) = (4, 0)$ and setting $\mu = 0$, we find that $s_{\max,e}$ is the positive root of

$$s^2 + \frac{1}{6}K^2(K-1)s - \frac{1}{24}K^4(K-4)(K-7) = 0 \quad (3.35)$$

For large K , this asymptotes to $s_e \sim K^3 \frac{\sqrt{7}-1}{12}$. We now summarize the above discussion as follows.

Proposition 3.4. *The (K, q) ring with $q > 0$ is **energetically unstable** with respect to mode $(m, M) = (1, 0)$ when $s > s_{(1,0)}$, or equivalently, when $\Omega > 0$. The threshold $s = s_{(1,0)}$ corresponds to rotation rate $\Omega = 0$ so that such ring is energetically unstable when $\Omega < 0$.*

Suppose that $K \leq 7$. Then there exists $s_{\max,e}$ such that a ring is stable if and only if $0 < s < s_{\max,e}$. When $K/2 < q < K/\sqrt{2}$, $s_{\max,e} \leq s_{(0,1)} < s_{(1,0)}$. Table III reports $s_{\max,e}$ for small q .

Suppose that $K > 7$ and $q = 1$. Then the ring is energetically stable if and only if $s_{\min,e} \leq s \leq s_{\max,e}$ where $s_{\min,e} = s_{(4,0)}$ is the positive root of (3.35), corresponding to the mode $(m, M) = (4, 0)$, whereas $s_{\max,e} = s_{(1,0)}$, corresponding to the mode $(m, M) = (1, 0)$.

Suppose that $K > 7$ and $q \neq 1$. Then the ring is energetically unstable.

Let us contrast dynamical and energetic stability. When $K \leq 7$, the ring is dynamically stable for all q and s . On the other hand, it is energetically stable only within the range $0 < s < s_{\max,e}$ as given in Table III. When $K > 7$ and $q \neq 1$, the ring is always energetically unstable. However it can be dynamically stable for $s > s_{\min,d}$ as long as $\gcd(K, q) = 1$; see Table II. Finally when $K > 7$ and $q = 1$, the ring is energetically stable only in the range $s_{\min,e} \leq s \leq s_{\max,e}$ whereas it is dynamically stable in the range $s_{\min,d} \leq s$. Table III gives a comparison between $s_{\min,e}$ and $s_{\min,d}$. Although not equal, these values are close to each other (within 9% for large K).

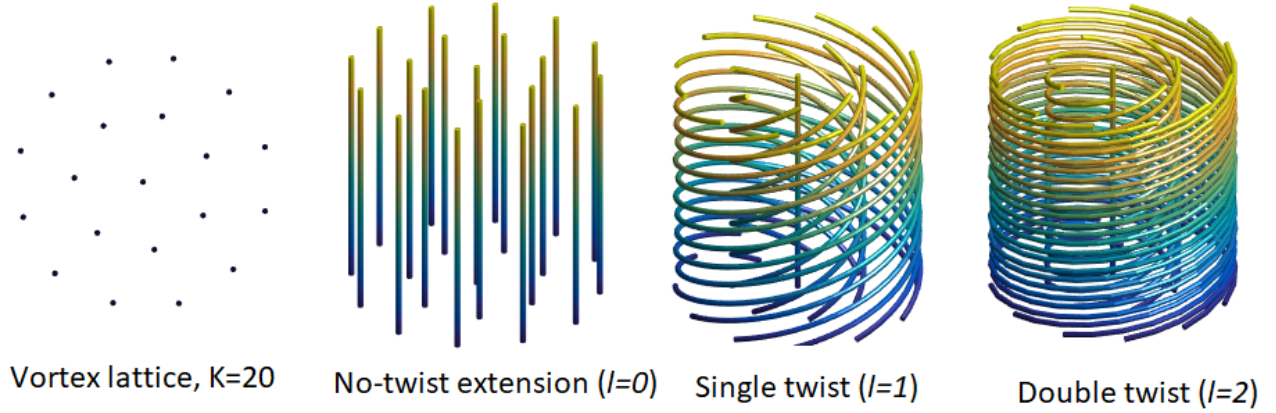


FIG. 3. Left: stable vortex lattice with 20 point vortices, corresponding to the stable steady state of (4.37). The remaining panels show the extension of this crystal to helical filament crystal with zero, 1 and 2 twists.

4. HELICAL FILAMENT LATTICE

Consider *any* relative equilibrium of point vortices η_k^0 satisfying (2.8). Then $\xi_k(z) = e^{zi\omega} \eta_k^0$ corresponds to a filament equilibrium satisfying (2.4) with a shifted frequency $\Omega = \Gamma - D\omega^2$. Moreover assume periodic boundary conditions, so that

$$\omega = \frac{2\pi}{P}l \text{ for an integer } l. \quad (4.36)$$

We refer to such configurations as helical filaments with l twists.

Suppose that the underlying vortex equilibrium is *energetically stable in the x - y plane*. In other words, η_k^0 is a *stable* equilibrium of the system

$$\frac{d}{dt}\eta_k = -\Gamma\eta_k + \sum_{j \neq k} \frac{\eta_k - \eta_j}{|\eta_k - \eta_j|^2}. \quad (4.37)$$

A relevant question then is what can be said, in general, about the associated 3D helical extension in terms of stability. By analogy to vortex crystals, we refer to such filament configurations as helical filament crystals. An example of a vortex crystal consisting of 20 vortices and its extensions are shown in Figure 3. We show the following result.

Theorem 4.1. *Let η_k^0 be a **stable** equilibrium of the system (4.37). Let $\xi_k = \exp(\omega iz) \eta_k^0$ be the corresponding twisted filament relative equilibrium satisfying*

$$0 = D \frac{\partial^2}{\partial z^2} \xi_k - \Omega \xi_k + \sum_{j \neq k} \frac{\xi_k - \xi_j}{|\xi_k - \xi_j|^2} \quad (4.38)$$

where $\Gamma = D\omega^2 + \Omega > 0$. Assume periodic boundary conditions for $z \in [0, P]$, so that $\omega = \frac{2\pi}{P}l$, $l \in \mathbb{Z}$. We have the following:

- ξ_k is energetically stable (i.e. stable with respect to (2.5)) if and only if $\Omega > \Omega_{\min, e}$ where

$$\Omega_{\min, e} := D \left(\frac{2\pi}{P} \right)^2 \left(l^2 - \frac{1}{2} \right). \quad (4.39)$$

- ξ_k is dynamically stable (i.e. stable with respect to (2.3)) for all Ω .

Note that Ω could be negative as long as $\Gamma > 0$. The latter condition is necessary for the steady state to exist, see (2.9). Before showing 4.1, we will need the following lemma.

Lemma 4.2. Let η_k^0 be a **stable** equilibrium of the system (4.37). Let $\phi = (\phi_1, \dots, \phi_K)$ and define the operator

$$L\phi = \sum_{j \neq k} \frac{-1}{(\bar{\eta}_k^0 - \bar{\eta}_j^0)^2} (\phi_k - \phi_j). \quad (4.40)$$

Suppose that μ is an eigenvalue of $\bar{L}L$, where \bar{L} involves taking a conjugate of Eq. (4.40), i.e. $\bar{L}\phi = \sum_{j \neq k} \frac{-1}{(\eta_k^0 - \eta_j^0)^2} (\phi_k - \phi_j)$. Then μ satisfies $0 \leq \mu \leq \Gamma^2$. Moreover, the maximum is achieved: there is an eigenvalue $\mu = \Gamma^2$ of $\bar{L}L$.

Proof of Lemma 4.2. First, note that L is symmetric so that $\bar{L}L$ is positive definite and hence all of its eigenvalues $\mu \geq 0$. To see that $\max \mu = \Gamma^2$, we linearize (4.37) around the equilibrium as $\eta_k(t) = \eta_k + e^{\kappa t} \phi_k$ to obtain the problem

$$(\kappa + \Gamma)\phi = L\bar{\phi}. \quad (4.41)$$

where L is given by (4.40), and κ is the eigenvalue of the linearization of (4.37). Taking a conjugate, we have

$$(\bar{\kappa} + \Gamma)\bar{\phi} = \bar{L}\phi.$$

Applying \bar{L} to both sides of (4.41) yields

$$|\kappa + \Gamma|^2 \bar{\phi} = \bar{L}L\bar{\phi} \quad (4.42)$$

Since (4.37) is the gradient flow of the associated energy $E = -\Gamma \sum_k \frac{|\eta_k|^2}{2} + \sum \sum_{j \neq k} \log |\eta_k - \eta_j|$, the relevant eigenvalues κ are all purely real. Therefore we have

$$(\kappa + \Gamma)^2 \bar{\phi} = \bar{L}L\bar{\phi}. \quad (4.43)$$

It follows that $(\kappa + \Gamma)^2 = \mu$ for some eigenvalue μ of $\bar{L}L$. Conversely, the matrix $\bar{L}L$ has K eigenvalues whereas the linearization of problem (4.37) has $2K$ eigenvalues. Therefore $\kappa = -\Gamma \pm \sqrt{\mu}$ are both eigenvalues of the linearization of Eq. (4.37) for any given eigenvalue μ of $\bar{L}L$. Given the stability assumption above for η_k^0 , it follows that $\kappa = -\Gamma \pm \sqrt{\mu} \leq 0$ or $\mu \leq \Gamma^2$. Finally, the problem (4.37) admits a zero eigenvalue $\kappa = 0$ corresponding to rotation invariance, so that $\mu = \Gamma^2$ is the maximum eigenvalue of $\bar{L}L$. ■

Proof of Proposition 4.1. We first prove (a). Linearize equations (2.5) as

$$\xi_k(z, t) = \xi_k(z) + \phi_k(z, t), \quad \phi_k \ll 1 \quad (4.44)$$

to obtain

$$(\partial_t + \Omega - D\partial_{zz})\phi = e^{2i\omega z} L\bar{\phi} \quad (4.45)$$

where $\phi = (\phi_1, \dots, \phi_K)^T$ and L is the linear operator (4.40).

Next we use the following ansatz:

$$\phi = \phi_+(t)e^{i(\omega+\alpha)z} + \bar{\phi}_-(t)e^{i(\omega-\alpha)z}.$$

to obtain

$$(\partial_t + \Omega + D(\omega + \alpha)^2)\phi_+ = L\phi_-; \quad (\partial_t + \Omega + D(\omega - \alpha)^2)\bar{\phi}_- = L\bar{\phi}_+; \quad (4.46)$$

Taking complex conjugate of the second equation we get

$$(\partial_t + \Omega + D(\omega - \alpha)^2)\phi_- = \bar{L}\phi_+. \quad (4.47)$$

Finally we take

$$\phi_{\pm} = e^{\lambda t} \varepsilon_{\pm} \quad (4.48)$$

to obtain

$$(\lambda + \Omega + D(\omega + \alpha)^2)\varepsilon_+ = L\varepsilon_-, \quad (\lambda + \Omega + D(\omega - \alpha)^2)\varepsilon_- = \bar{L}\varepsilon_+.$$

We apply \bar{L} to the first equation to obtain

$$\left(\lambda + D(\omega + \alpha)^2 + \Omega\right) \left(\lambda + D(\omega - \alpha)^2 + \Omega\right) = \mu \quad (4.49)$$

where μ is eigenvalue of $\bar{L}L$. In terms of Γ this becomes

$$\lambda^2 + 2\lambda(\alpha^2 + \Gamma) + D\alpha^2(D\alpha^2 - 4D\omega^2 + 2\Gamma) + \Gamma^2 - \mu = 0. \quad (4.50)$$

Therefore a necessary and sufficient condition for stability is that $D\alpha^2(D\alpha^2 - 4d\omega^2 + 2\Gamma) + \Gamma^2 - \mu \geq 0$ for all admissible α, μ . By Lemma 4.2, $0 \leq \mu \leq \Gamma^2$ with $\max \mu = \Gamma^2$. So the stability condition becomes $D\alpha^2(D\alpha^2 - 4d\omega^2 + 2\Gamma) \geq \max(\mu) - \Gamma^2 = 0$. Upon substituting $\Gamma = D\omega^2 + \Omega$, this is equivalent to $D\alpha^2 - 2D\omega^2 + 2\Omega \geq 0$, or $\Omega \geq \max_{\alpha, \alpha \neq 0} D\left(\omega^2 - \frac{\alpha^2}{2}\right)$. This is maximized when $M = \pm 1$, $\alpha = 2\pi/P$, showing (4.39).

We now show part (b). Linearizing (2.5) in the same way as part (a), we obtain

$$\begin{aligned} (-i\partial_t + \Omega + D(\omega + \alpha)^2)\phi_+ &= L\phi_-; \\ (i\partial_t + \Omega + D(\omega - \alpha)^2)\phi_- &= \bar{L}\phi_+. \end{aligned}$$

and instead of (4.49) we obtain

$$\left(-i\lambda + D(\omega + \alpha)^2 + \Omega\right) \left(i\lambda + D(\omega - \alpha)^2 + \Omega\right) = \mu \quad (4.51)$$

so that λ satisfies

$$\lambda^2 + i\lambda 4D\omega\alpha + D\alpha^2(D\alpha^2 - 4D\omega^2 + 2\Gamma) + \Gamma^2 - \mu = 0. \quad (4.52)$$

After some algebra we obtain

$$\lambda = \left(-2D\omega\alpha \pm \sqrt{D\alpha^2(D\alpha^2 + 2\Gamma) + \Gamma^2 - \mu}\right) i$$

By Lemma 4.2, $\mu < \Gamma^2$ so the expression under the square root is always positive. This shows that λ is purely imaginary for all parameter values which proves dynamical stability. ■

Example: filament ring. First, we verify that this result agrees with stability of ring solutions, refer to Figure 4. For periodic solutions, $l = q/K$ must be an integer. For example, take $K = 6, q = 6$; from table II; we read the threshold of $s_{\max, e} = 3.33$. Recalling (2.14, 3.26), we have $\Omega = \frac{2\pi}{P} D \left(\frac{K-1}{s} - \frac{q^2}{K^2} \right) = D \left(\frac{2\pi}{P} \right)^2 \cdot 0.50$. This corresponds precisely to (4.39) with $l = 1 = q/K$. Numerical simulations with $D = 0.5, P = 2\pi, \Omega = 0.24$ are shown in Figure 4 (top). For this value, $\Omega < \Omega_{\min, e} = 0.25$ and as expected, an instability is observed. This instability leads to a finite-time ‘‘collapse’’ around $t \approx 339.5$, corresponding to the crossing of the filaments. Continuing numerical simulations of (2.3) beyond this collapse leads to another (stable) ring, this time with $l = 0$.

Example: crystal filament lattice. For more than 7 point vortices, the energetically preferred state is a ‘‘lattice’’ such as shown in Figure 3. As in the preceding example, taking $P = 2\pi, D = 1/2$, we find that $\Omega_{\min} = 0.25$ when $l = 1$ (indeed Ω_{\min} only depends on l and not on the number of filaments). Simulation of (2.3) with $\Omega = 0.26$ and $l = 1$ exhibits a stable state. On the other hand, decreasing $\Omega = 0.24$ results in an instability of the $l = 1$ lattice, as illustrated in Figure 4.

We remark that Ω_c is always positive since $\omega \geq 2\pi/P$. Note that the more twisted (bigger ω) the configuration is, the bigger the rotation Ω should be to stabilize it. Also for an infinitely long filament ($P = \infty$), the equation (4.39) reduces to $\Omega_{\min} = 0$.

5. COMPARISON TO FULL NUMERICAL SIMULATIONS OF GP EQUATIONS

In this section we discuss our simulations of the full solution of the governing GP PDE in 3D. Recall that the latter is the natural starting point for deriving the KMD model, as discussed, e.g., in [38]. The GP equation reads:

$$i \frac{d\psi}{dt} = -\frac{1}{2} \nabla^2 \psi + V(R)\psi + g|\psi|^2\psi. \quad (5.53)$$

Here $g = 4\pi Na/l_R$ and a is the s-wave scattering, l_R is the axial oscillator length: $\sqrt{\hbar/m\omega_R}$ with R being the axial coordinate ($R^2 = x^2 + y^2$), m is the atomic mass, and ω_R is the axial trap frequency. In our simulations we have rescaled the length by l_R , time by $1/\omega_R$ and the energy by $\hbar\omega_R$ to get the form in (5.53). Throughout

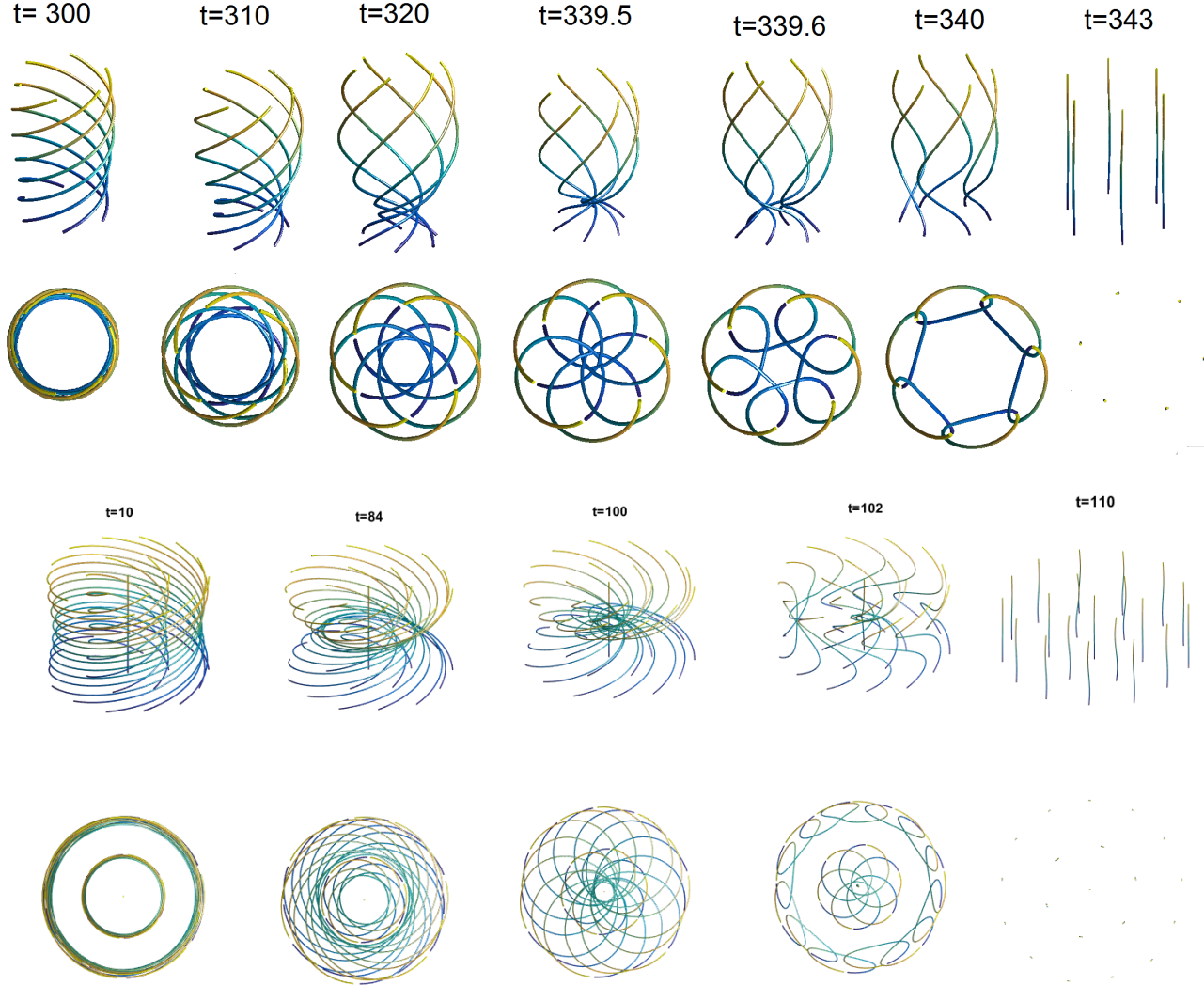


FIG. 4. Top: Simulations of (2.3) starting with a ring $(K, q) = (6, 6)$ and with $D = 0.5$, $\Omega = 0.24$. Instability is observed, followed by a finite-time collapse as the filaments cross each-other. Continuing the simulation after the collapse leads to a stable ring of straight filaments. Bottom: Simulations of (2.3) with $K = 20$ filaments and with initial conditions as in Figure 3 with $l = 1$. The remaining parameters are the same as above.

this manuscript, we work in these scaled dimensions which are tantamount to the dimensions used in the reduced system of Eq (2.1). This affords us the opportunity to connect our results to those of the full 3D field theory. The vortex lines (constituting the filaments of our effective filament model) are topological defects in the complex order parameter of the GP theory on which there is a vanishing of the density ($|\psi|$) and around which a suitable winding of the phase takes place. It is via these features that we identify and visualize the vortex filaments in the numerical results described below.

As our choice of trapping for $V(R)$, we simulated both an axial harmonic trap ($\frac{1}{2}R^2 = \frac{1}{2}(x^2 + y^2)$) and a flat bottom trap. We present the flat bottom trap results to remove the effect of an inhomogeneous background density profile. This potential has harmonic confinement beyond R_0 , so $V(R) = 1/2(R - R_0)^2\Theta(R - R_0)$ where $\Theta(x)$ is a Heaviside function that is 1 when $x \geq 0$ and zero otherwise. We have picked $R_0 = 4$, and we have tested that this does not influence vortex motion when they are well within this radius (i.e., for $R \leq 2$).

The chemical potential μ is chosen to be large ($30-42 \hbar\omega_r$), so this gives a small healing length, ξ , as $1/\sqrt{\mu}$. In addition to r (the ring filament radius) and P (the size of the domain along the z axis), the healing length defines a scale in the simulation which complicates the comparison with the filament method. We have picked the r to be in the range of 1-2, so it is much larger than ξ and much smaller than R_0 . This range of r usually means that the initial separation between vortex filaments is much larger than ξ and hence the latter scale does not have a critical

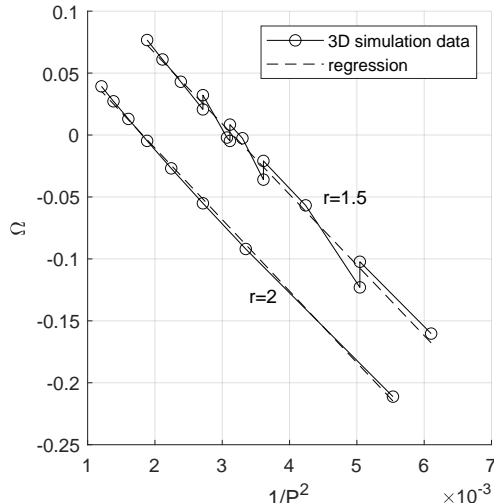


FIG. 5. Comparison of the full simulation of (5.53) and the theory (of Eq. (2.14)). Simulations are done for $(K, q) = (2, 2)$ ring with fixed r (either $r = 1$ or $r = 2$), and for several values of box height P , and the resulting rotation rate Ω is then recorded. The theory of Eq. (2.14) predicts a linear relationship between Ω and P^{-2} which is verified in the direct numerical computations of the 3D GP PDE of Eq. (5.53).

role in the dynamics.

The time propagation of Eq.(5.53) takes place with a third-order operator splitting Fourier spectral method using time steps of 5×10^{-4} . The spatial grid has 128^3 points and with a grid spacing of $0.15l_R$ in x and y , while dz is varied to get a desired P . We used periodic boundary conditions for all simulations of the vortex twists. We find the initial condition by first imprinting the phase with the ansatz:

$$\psi(x, y, z)/|\psi| = \Pi_j \tan^{-1}(x - x_j, y - y_j), \quad (5.54)$$

where x_j, y_j is the position of the j -th vortex core. Thus, the total phase is simply the sum of all the vortex core phases. After the phase is defined, we evolve ψ in imaginary time to relax the density. Once the energy changes by less than $10^{-8}\hbar\omega_r$, we consider the initial condition converged. The phase imprinting locks the vortices in place, and only the density is changed at this stage, so the configuration (to which the dynamics locks) can be metastable.

To find stationary states in the full simulations we must vary the simulation box height. An example of this is shown in Fig. 5, where we show plot the rotational velocity of the vortex twist as a function of $1/P^2$. Here we can see that Ω (measured in radians per trap unit of time) crosses zero at a particular value of $1/P^2$. In addition, for $r=1.5$, we show the extracted data from simulations with two different chemical potentials, 30 and 42 $\hbar\omega_R$. KMD theory predicts that Ω is a linear function of $1/P^2$, see (2.14). This is validated with full GP simulations as seen in Fig. 5.

We now consider three illustrative examples of for $K = 2, 3$, and 4 with $q = K$.

For $K = 2$ and 3, we were able to find the P that essentially froze the motion of the vortices. In these figures, the 3D vortex cores are shown as red lines. The vortex positions are extracted by finding the phase singularity on the computational grid [51]. We refine the vortex positions using methods from Refs. [52, 53]. We also project the vortex core positions on the sides of the figure. Additionally, we have shown the projected density of the BEC projected as thin contours on the sides of the figure. Figure 6 shows the full simulations for $K = 2, 3$ with $q = K$. Such a filament ring appears to be stable (and practically stationary) regardless of the initial radius r . This is in agreement with the results in Section 3.3.1, which show that such a ring is dynamically stable for all parameters (even though it may be energetically unstable, see Section 2). Recall that the Hamiltonian GP model of Eq. (5.53) is connected at a reduced level with the KMD filament setting of Eq. (2.1) (rather than with the gradient dynamics of Eq. (2.5)).

Figure 7 shows the full simulations with $K = 4, q = 4$. The simulation is initially stationary, but eventually the vortex twist gains a collective motion that is depicted in the snapshots. This destabilizes the configuration which is apparently dynamically unstable. Additionally in Figure 7(f), we show the same vortex configuration with slight perturbations on the initial condition. The end result is that the system never appears stationary and has a much more disordered appearance. Indeed, what we expect here is that the correspondence between the KMD filament model and the complex 3D dynamics of the GP of Eq. (5.53) may break down as one goes to a regime involving a

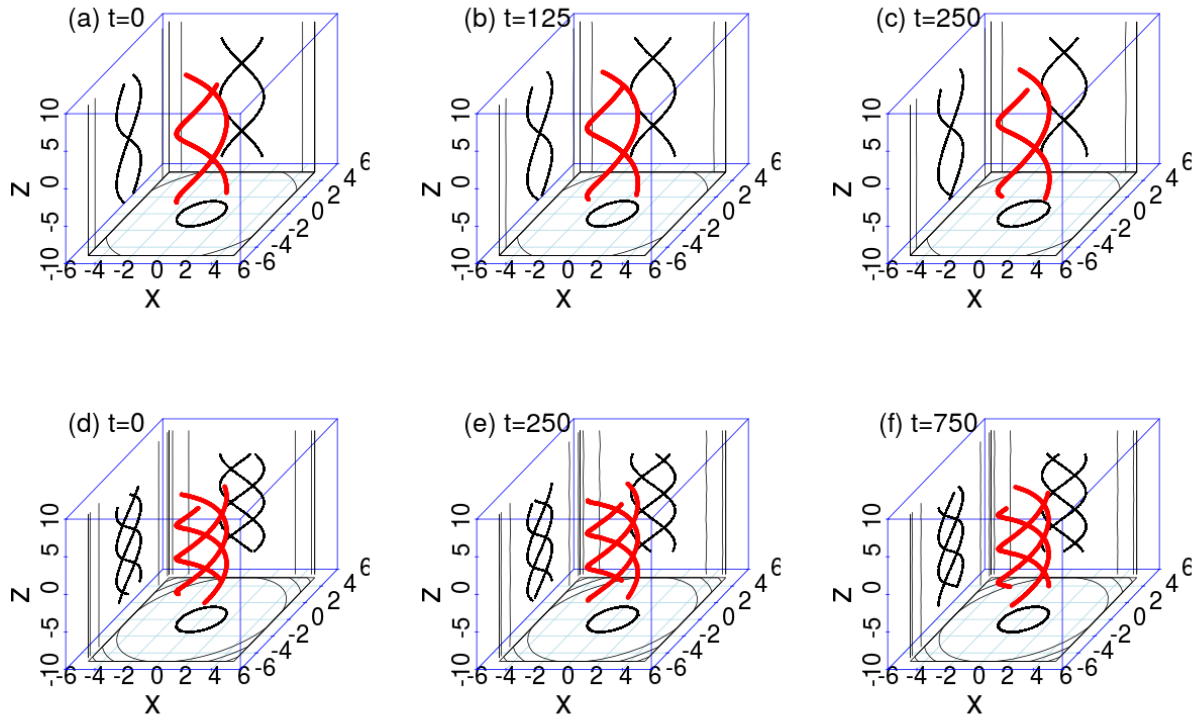


FIG. 6. For $K = 2$ (top) and $K = 3$ (bottom), the vortices appear stable and are very nearly stationary. For $K = 2$, the times in trap units are (a) 0, (b) 125, and (c) 250. For $K = 3$, the simulations were run for 1.5 million time steps, three times longer than usual, to test stability. The times shown are (d) 0, (e) 500 and (f) 750 in trap units. The vortices are shown as red points and their project is seen in the side as bold black points. The projected density contours are shown as thin black lines on the sides.

large number of filaments rotating at small distances from one another. Nevertheless, we believe that the above select examples suggest the analysis of the KMD model as a useful tool for identifying multi-vortex-filament configurations in the original PDE system of relevance to a wide range of (e.g., atomic, optical and hydrodynamic) applications.

6. DISCUSSION

Our aim in the present work was to explore the dynamical reduction afforded by the KMD model in order to propose exact, analytically tractable solutions at the level of multiple vortex filaments (in particular, filament rings and lattices). Moreover, this reduced description enabled a systematic characterization of the stability of such states both at the level of dynamical stability (of the original Hamiltonian problem), as well as at that of energetic stability (relevant to the gradient flow of Eq. (2.5)). We illustrated that while the more stringent conditions for energetic stability imply dynamical stability, the converse is false. The relevant conditions of stability for the vortex filaments depend on the number of filaments (and the relevant periodicity) with, e.g., $K \leq 7$ leading to dynamical stability. On the other hand, for the helical filament lattices we could establish that the configuration is dynamically stable provided that the underlying vortex configuration is energetically stable in the two-dimensional plane. We have gone on to explore some prototypical ones among these results in a fully 3-dimensional simulation of the original Gross-Pitaevskii model from which the filament KMD reduction was obtained. We have seen that in some of the simpler settings involving e.g. 2 or 3 filaments, the results of the 3D simulation are in line with those of the reduced case. However, for larger numbers of filaments, we found potential instabilities in the original model that were not mirrored in the reduction. A systematic exploration of the breakdown of the model for larger numbers of filaments is a particularly interesting topic for future study.

Naturally, there are numerous directions that our study paves towards future work. For instance, one possibility that we have touched upon and which is illustrated in Figure 8 for $K = 20$, $q = 1$ is to use D as the bifurcation parameter (while we fix $\Omega = 1$). In that case, we find that the energetic stability boundaries appear to be supercritical

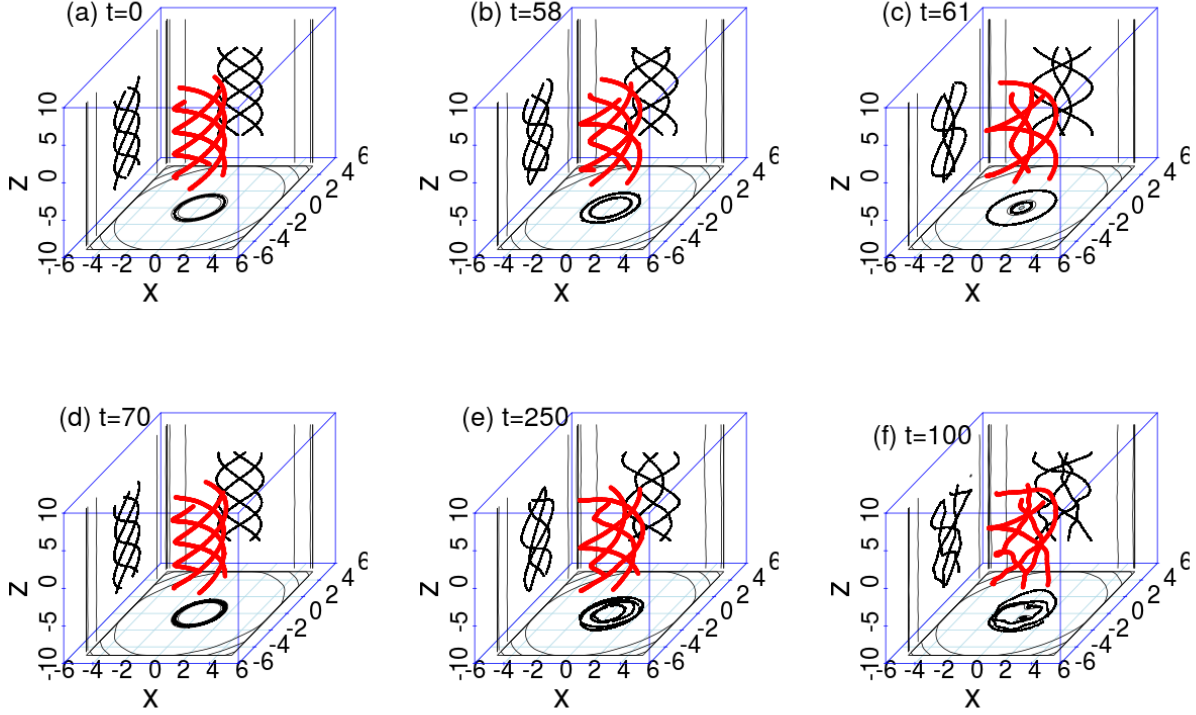
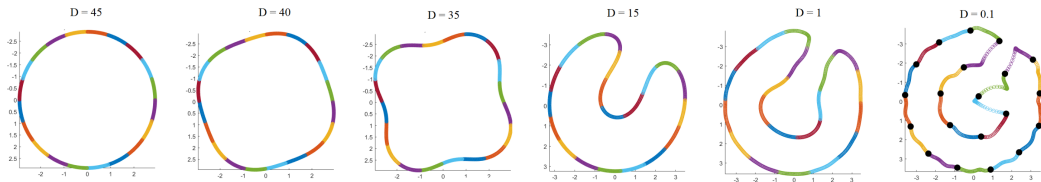


FIG. 7. For $K = 4$, the vortices initially appear to be stationary, but then a collective motion breaks out and the vortex configuration scrambles. The times shown are (a) 0, (b) 58, (b) 61, (d) 70, and (e) 250 in trap units. (e) The last snapshot is the same configuration with perturbations on the initial position of the vortices and because of these it quickly evolves out of the initial configuration. For this simulation the time shown is 100.

FIG. 8. Energetically stable configurations of a single vortex filament wrapped around 20 times (so that $K = 20, \xi_k(P) = \xi_{k+1 \bmod K}(0)$). The figure shows the view looking down the z -axis (i.e. the projection onto x - y plane). Here, $\Omega = 1$ and $P = 2\pi$ with D as indicated. Each snapshot corresponds to the numerically computed steady state of (2.5). For large D ($D > D_{\min} = 40.8$), the steady state is a ring-like configuration. For small D , most x - y cross-sections show a 2D vortex crystal structure.



and can lead to bifurcations of novel nearby stable equilibria. For this particular example, the thresholds $s_{\min,e} = 703.7$, $s_{\max,e} = 7600$ (from Table III) then correspond to $D = 40.8$ and $D = \infty$, respectively. As D is decreased past 40.8, a mode-4 instability destabilizes the ring. This instability appears to be supercritical: while the ring is energetically unstable, a nearby mode-4 pattern appears to be stable, and the system converges to it. As D is decreased further, subsequent bifurcations are observed. In the limit $D \rightarrow 0$, the various z -cross-sections decouple and each cross-section looks like a point vortex lattice; these layers are connected through sharp transitions. Numerical experiments suggest that bifurcations in Figure 8 are reversible: as D is increased, the steady state straightens itself out, eventually resulting in a single ring. Our numerical experiments suggest the following conjecture worth pursuing in future studies:

Conjecture 6.1. *For boundary conditions $\xi_k(P) = \xi_{k+1 \bmod K}(0)$ in the limit $D \rightarrow \infty$, the only energetically stable equilibrium is the $q = 1$ ring.*

Furthermore, there are numerous open questions related to filament interactions and non-equilibrium solutions; see, e.g., [54] for some recent results on two-filament interactions. But even for equilibrium states, a whole zoo of

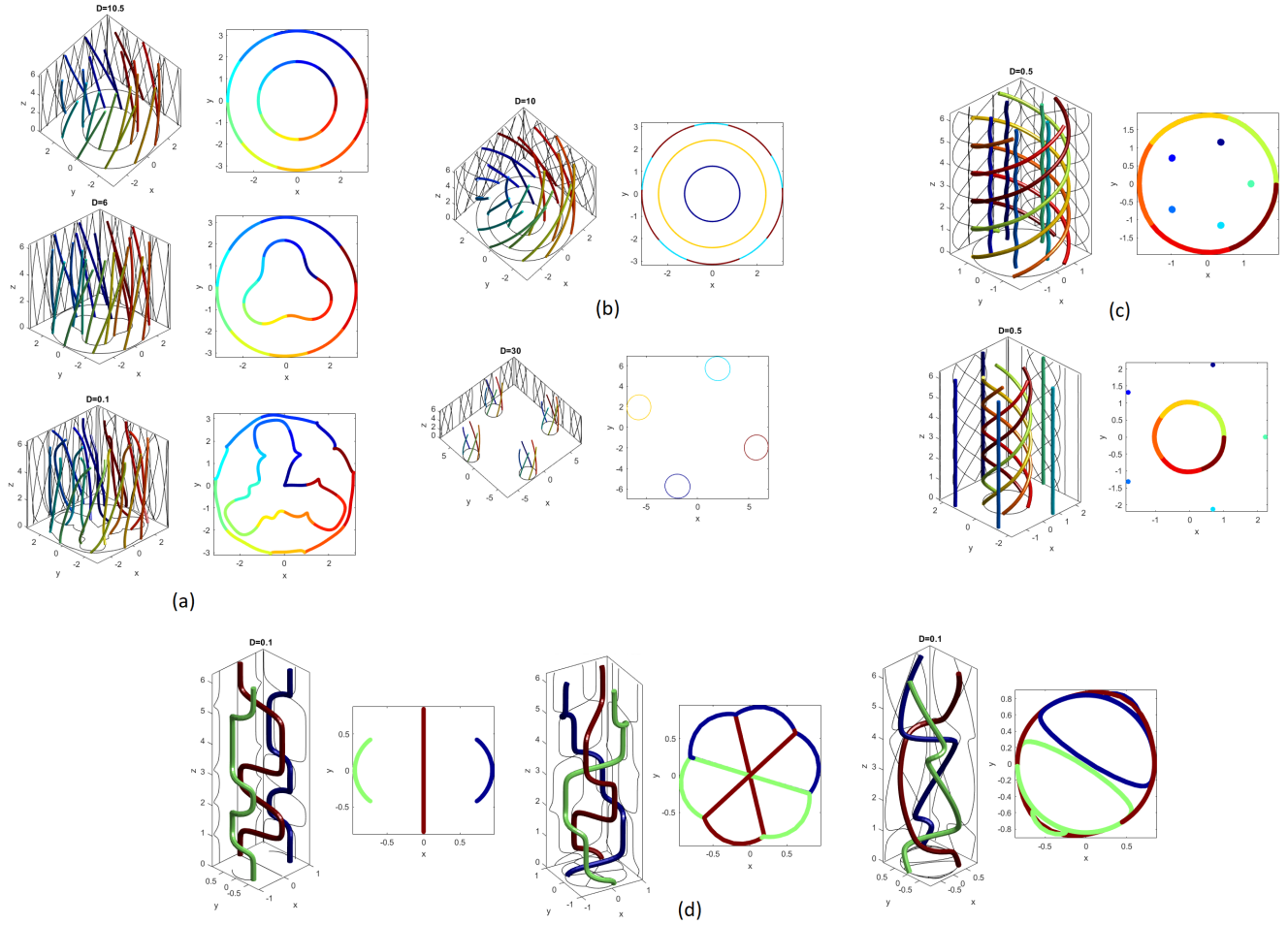


FIG. 9. A selection of non-helical energetically stable relative equilibria obtained by solving (2.5) numerically. (a) Initial conditions consist of a helical ring $(K, q) = (20, 2)$ and converge to a double-ring solution when $D = 10$. A cascade of bifurcations is observed as D is decreased. (b) Taking initial conditions $(K, q) = (20, 4)$ with $D = 10$ and $D = 30$. Note the “triple-ring” solution. (c) Mixed helical state (d) Three filaments with $D = 0.1$, starting from different initial conditions. The resulting states exhibit high symmetry and sharp boundary layers.

other “exotic” (non-helical) relative equilibria exist, as illustrated in Figure 9 in connection to the gradient flow of Eq. (2.5). In this figure, we observe different types of energetically stable equilibria resulting from initial conditions with different combinations of (K, q) , for a few distinct values of D . The helical states we considered in this paper only scratch the surface of what is possible and provide a sense of the wealth of associated possibilities. Understanding the emergence/bifurcations of such states, but also the energy landscape and dynamics associated with them provide, in our view, a fascinating potential for further exploration.

-
- [1] L. Pismen, *Vortices in Nonlinear Fields*, Oxford University Press, Clarendon, UK, 1999.
 - [2] R. Donnelly, *Quantized Vortices in Helium II*, Cambridge University Press, Cambridge, UK, 1991.
 - [3] G. Blatter, M. V. Feigel'man, V. B. Geshkenbein, A. I. Larkin, V. M. Vinokur, *Vortices in high-temperature superconductors*, *Rev. Mod. Phys.* 66 (1994) 1125–1388.
 - [4] P. Saffman, *Vortex Dynamics*, Cambridge University Press, Cambridge, UK, 1992.
 - [5] L. Pitaevskii, S. Stringari, *Bose–Einstein Condensation*, Oxford University Press, Oxford, UK, 2003.
 - [6] C. Pethick, H. Smith, *Bose–Einstein Condensation in Dilute Gases*, Cambridge University Press, Cambridge, UK, 2002.
 - [7] P. Kevrekidis, D. Frantzeskakis, R. Carretero-González, *The Defocusing Nonlinear Schrödinger Equation*, Society for Industrial and Applied Mathematics, Philadelphia, PA, 2015.
 - [8] A. L. Fetter, *Rotating trapped bose-einstein condensates*, *Rev. Mod. Phys.* 81 (2009) 647–691.

- [9] A. L. Fetter, A. A. Svidzinsky, Vortices in a trapped dilute bose-einstein condensate, *Journal of Physics: Condensed Matter* 13 (12) (2001) R135.
- [10] P. Kevrekidis, R. Carretero-González, D. Frantzeskakis, I. Kevrekidis, Vortices in bose-einstein condensates: some recent developments, *Modern Physics Letters B* 18 (30) (2004) 1481–1505.
- [11] S. Komineas, Vortex rings and solitary waves in trapped bose-einstein condensates, *The European Physical Journal Special Topics* 147 (1) (2007) 133–152.
- [12] A. C. White, B. P. Anderson, V. S. Bagnato, Vortices and turbulence in trapped atomic condensates, *Proceedings of the National Academy of Sciences* (2014).
- [13] M. C. Tsatsos, P. E. Tavares, A. Cidrim, A. R. Fritsch, M. A. Caracanhas, F. E. A. dos Santos, C. F. Barenghi, V. S. Bagnato, Quantum turbulence in trapped atomic bose-einstein condensates, *Physics Reports* 622 (2016) 1 – 52, quantum turbulence in trapped atomic Bose-Einstein condensates.
- [14] R. Ricca, D. Samuels, C. Barenghi, Evolution of vortex knots, *Journal of Fluid Mechanics* 391 (1999) 29–44.
- [15] F. Maggioni, S. Alamri, C. F. Barenghi, R. L. Ricca, Velocity, energy, and helicity of vortex knots and unknots, *Phys. Rev. E* 82 (2010) 026309.
- [16] F. Maggioni, S. Alamri, C. F. Barenghi, R. L. Ricca, Velocity, energy, and helicity of vortex knots and unknots, *Phys. Rev. E* 82 (2010) 026309.
- [17] D. Kleckner, W. Irvine, Creation and dynamics of knotted vortices, *Nature Phys.* 9 (2013) 253–258.
- [18] D. Proment, M. Onorato, C. F. Barenghi, Torus quantum vortex knots in the gross-pitaevskii model for bose-einstein condensates, *Journal of Physics: Conference Series* 544 (2014) 012022.
- [19] P. Clark di Leoni, P. D. Mininni, M. E. Brachet, Helicity, topology, and kelvin waves in reconnecting quantum knots, *Phys. Rev. A* 94 (2016) 043605.
- [20] D. Kleckner, W. Kauffman, L.H. Irvine, How superfluid vortex knots untie, *Nature Phys.* 12 (2016) 650–655.
- [21] V. P. Ruban, Long-lived quantum vortex knots, *JETP Letters* 107 (5) (2018) 307–310.
- [22] V. P. Ruban, Quasi-stable configurations of torus vortex knots and links, *Journal of Experimental and Theoretical Physics* 127 (3) (2018) 581–586.
- [23] C. Ticknor, V. P. Ruban, P. G. Kevrekidis, Quasistable quantum vortex knots and links in anisotropic harmonically trapped bose-einstein condensates, *Phys. Rev. A* 99 (2019) 063604.
- [24] D. Hall, M. Ray, K. Tiurev, R. E., A. Gheorghie, M. Möttönen, Tying quantum knots, *Nature Phys.* 12 (2016) 478–483.
- [25] W. Lee, A. H. Gheorghie, K. Tiurev, T. Ollikainen, M. Möttönen, D. S. Hall, Synthetic electromagnetic knot in a three-dimensional skyrmion, *Science Advances* 4 (3) (2018).
- [26] A. Desyatnikov, D. Buccoliero, M. Dennis, Y. Kivshar, Spontaneous knotting of self-trapped waves, *Sci. Rep.* 2:771 (2012) 1–7.
- [27] K. Shimokawa, K. Ishihara, I. Grainge, D. J. Sherratt, M. Vazquez, Ftsk-dependent xercd-dif recombination unlinks replication catenanes in a stepwise manner, *Proceedings of the National Academy of Sciences* 110 (52) (2013) 20906–20911.
- [28] J. Cirtain, L. Golub, A. Winebarger, B. De Pontieu, K. Kobayashi, R. Moore, R. Walsh, K. Korreck, M. Weber, P. McCauley, T. A., S. Kuzin, D. C.E., Energy release in the solar corona from spatially resolved magnetic braids, *Nature* 493 (2013) 501–503.
- [29] T. Lim, On the role of kelvin-helmholtz-like instability in the formation of turbulent vortex rings, *Fluid dynamics research* 21 (1) (1997) 47–56.
- [30] R. Caplan, J. Talley, R. Carretero-González, P. Kevrekidis, Scattering and leapfrogging of vortex rings in a superfluid, *Physics of Fluids* 26 (9) (2014) 097101.
- [31] A. W. Baggaley, C. F. Barenghi, Spectrum of turbulent kelvin-waves cascade in superfluid helium, *Physical Review B* 83 (13) (2011) 134509.
- [32] V. Okulov, J. N. Sørensen, Maximum efficiency of wind turbine rotors using joukowsky and betz approaches, *Journal of Fluid Mechanics* 649 (2010) 497–508.
- [33] V. Okulov, On the stability of multiple helical vortices, *Journal of Fluid Mechanics* 521 (2004) 319–342.
- [34] H. U. Quaranta, H. Bolnot, T. Leweke, Long-wave instability of a helical vortex, *Journal of Fluid Mechanics* 780 (2015) 687–716.
- [35] T. Leweke, H. Quaranta, H. Bolnot, F. Blanco-Rodríguez, S. Le Dizès, Long-and short-wave instabilities in helical vortices, in: *Journal of Physics: Conference Series*, Vol. 524, IOP Publishing, 2014, p. 012154.
- [36] R. Klein, A. J. Majda, K. Damodaran, Simplified equations for the interaction of nearly parallel vortex filaments, *Journal of Fluid Mechanics* 288 (1995) 201–248.
- [37] P.-L. Lions, A. Majda, Equilibrium statistical theory for nearly parallel vortex filaments, *Communications on Pure and Applied Mathematics: A Journal Issued by the Courant Institute of Mathematical Sciences* 53 (1) (2000) 76–142.
- [38] A. Contreras, R. L. Jerrard, Nearly parallel vortex filaments in the 3d ginzburg-landau equations, *arXiv preprint arXiv:1606.00732* (2016).
- [39] A. Barry, G. Hall, C. Wayne, Relative equilibria of the $(1+n)$ -vortex problem, *Journal of nonlinear science* 22 (1) (2012) 63–83.
- [40] P. Newton, *The N-vortex problem: analytical techniques*, Vol. 145, Springer, 2001.
- [41] H. Aref, P. Newton, M. Stremler, T. Tokieda, D. Vainchtein, Vortex crystals, *Advances in applied Mechanics* 39 (2003) 1–79.
- [42] J. Palmore, Relative equilibria of vortices in two dimensions, *Proceedings of the National Academy of Sciences* 79 (2) (1982) 716–718.
- [43] D. Yan, R. Carretero-González, D. J. Frantzeskakis, P. G. Kevrekidis, N. P. Proukakis, D. Spirn, Exploring vortex

- dynamics in the presence of dissipation: Analytical and numerical results, *Phys. Rev. A* 89 (2014) 043613.
- [44] T. I. Zueva, Dissipative motion of vortices in spatially inhomogeneous bose-einstein condensates, *Low Temperature Physics* 45 (1) (2019) 67–77.
 - [45] G. Moon, W. J. Kwon, H. Lee, Y.-i. Shin, Thermal friction on quantum vortices in a bose-einstein condensate, *Phys. Rev. A* 92 (2015) 051601.
 - [46] J. Ruostekoski, Z. Dutton, Dynamical and energetic instabilities in multicomponent bose-einstein condensates in optical lattices, *Phys. Rev. A* 76 (2007) 063607.
 - [47] Y. Chen, T. Kolokolnikov, D. Zhirov, Collective behaviour of large number of vortices in the plane, *Proceedings of the Royal Society A: Mathematical, Physical and Engineering Sciences* 469 (2156) (2013) 20130085.
 - [48] T. Kolokolnikov, P. Kevrekidis, R. Carretero-González, A tale of two distributions: from few to many vortices in quasi-two-dimensional bose–einstein condensates, *Proceedings of the Royal Society A: Mathematical, Physical and Engineering Sciences* 470 (2168) (2014) 20140048.
 - [49] T. Kolokolnikov, H. Sun, D. Uminsky, A. L. Bertozzi, Stability of ring patterns arising from two-dimensional particle interactions, *Phys. Rev. E Rapid. Comm.* 84 (2011) 015203.
 - [50] T. Havelock, Lii. the stability of motion of rectilinear vortices in ring formation, *The London, Edinburgh, and Dublin Philosophical Magazine and Journal of Science* 11 (70) (1931) 617–633.
 - [51] C. J. Foster, P. B. Blakie, M. J. Davis, Vortex pairing in two-dimensional bose gases, *Phys. Rev. A* 81 (2010) 023623.
 - [52] R. N. Bisset, S. Serafini, E. Iseni, M. Barbiero, T. Bienaimé, G. Lamporesi, G. Ferrari, F. Dalfovo, Observation of a spinning top in a bose-einstein condensate, *Phys. Rev. A* 96 (2017) 053605.
 - [53] A. Vilhois, G. Krstulovic, D. Proment, H. Salman, A vortex filament tracking method for the gross–pitaevskii model of a superfluid, *Journal of Physics A: Mathematical and Theoretical* 49 (41) (2016) 415502.
 - [54] J. A. Kwiecinski, R. A. Van Gorder, Dynamics of nearly parallel interacting vortex filaments, *Journal of Fluid Mechanics* 835 (2018) 575–623.